Refractive Index Susceptibility of the Plasmonic Palladium Nanoparticle: Potential as the Third Plasmonic Sensing Material

Kosuke Sugawa,[*,†] Hironobu Tahara,[*,‡] Ayane Yamashita,[†] Joe Otsuki,[†] Takamasa Sagara,[‡] Takashi Harumoto,[§] and Sayaka Yanagida[§]

[†]College of Science and Technology, Nihon University, Chiyoda, Tokyo 101-8308, Japan, [‡]Division of Chemistry and Materials Science, Graduate School of Engineering, Nagasaki University, Nagasaki 852-8521, Japan, and [§]Department of Material Science and Technology, Tokyo University of Science, Katsushika, Tokyo 125-8585, Japan

ABSTRACT We demonstrate that Pd nanospheres exhibit much higher susceptibility of the localized surface plasmon resonance (LSPR) peak to medium refractive index changes than commonly used plasmonic sensing materials such as Au and Ag. The susceptibility of spherical Au nanoparticle—core/Pd-shell nanospheres (Au/PdNSs, ca. 73 nm in diameter) was found to be 4.9 and 2.5 times higher, respectively, than those of Au (AuNSs) and Ag nanospheres (AgNSs) having similar diameters. The experimental finding was theoretically substantiated using the Mie exact solution. We also showed from a quasi-static (QS) approximation framework that the high susceptibility of Pd LSPR originates from the smaller dispersion of the real part of its dielectric function than those of Au and Ag LSPR around the resonant wavelength. We conclude that the Pd nanoparticle is a promising candidate of "the third plasmonic sensing material" following Au and Ag to be used in ultrahigh-sensitive LSPR sensors.

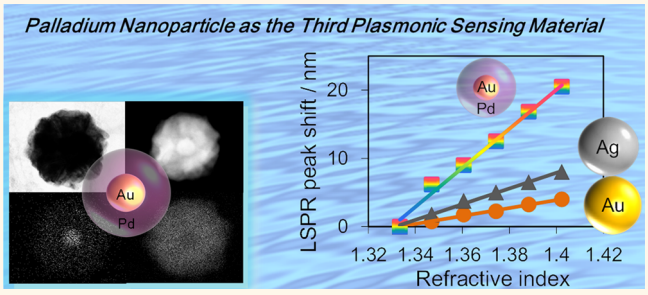

KEYWORDS: localized surface plasmon · palladium nanoparticles · refractive index susceptibility · core—shell nanoparticles · ultraviolet region

Metal nanoparticles have attracted much attention because of their unique optical properties, especially the emergence of localized surface plasmon resonance (LSPR), significantly different from bulk metals. The LSPR arises from collective oscillations of free electrons in the metal nanoparticles in resonance with incoming light fields, resulting in strong local electromagnetic fields as well as an intense extinction band.[1]

It is well-studied that an increase in the refractive index (RI) of the medium surrounding the plasmonic nanoparticles causes redshifts in the plasmon extinction band.[2] LSPR sensors based on the susceptibility of the LSPR peak position of plasmonic nanoparticles to the RI changes have been utilized to detect analytes. It is a promising technology for simple, label-free, and cost-effective real time optical sensing.[3,4] Indeed, applications of the LSPR sensing have been reported for immunoassay[5] and for the detection of various biomolecules including cancer biomarker,[6−8] DNA,[9,10] and so on. Recently, it has been reported that LSPR sensor could be utilized to detect hazardous or toxic gases.[11,12] The sensor can also be used to monitor catalytic reactions on Pt/BaO[13] and H_2 storage in palladium (Pd) nanoparticles.[14−20]

Gold (Au) and silver (Ag) nanoparticles have exclusively been used for the application to the sensor materials because of their high susceptibilities to RI changes in the surrounding media. To lower substantially the detection limit for low-molecular weight analytes, metal nanoparticles possessing higher RI susceptibilities are in high demand. It has already been demonstrated that the response to RI changes can be enhanced by optimizing nanoparticle shapes as well as the nanoparticle diameters.[21] Empirical studies

* Address correspondence to sugawa.kosuke@nihon-u.ac.jp, h-tahara@nagasaki-u.ac.jp.

Received for review November 29, 2014 and accepted January 28, 2015.

Published online January 28, 2015
10.1021/nn506800a

have shown that Au and Ag nanoparticles with various anisotropic shapes, including Au nanobranches,[22] Au nanorods,[22−24] Au nanobipyramids,[22] Au nanostars,[25] Au pyramids,[26] Au nanorattles,[27] Au nanoprisms,[28] Ag nanoprisms,[29,30] Ag nanocubes,[31] Au nanoframes,[32] Au nanoring,[33] Au/Pd octopods,[34] and Au nanoparticle dimers,[35] have inherently high RI susceptibilities because of their large surface charge polarizability. Also, the RI susceptibilities are strongly dependent on the metal species comprising the nanoparticles. Haes *et al.* reported that the LSPR from Ag triangular nanoplates showed larger RI sensitivities as compared with that from Au nanoplates of identical shapes and sizes.[36] In addition, another report demonstrated that the RI susceptibilities of LSPR of the dipole mode from Ag nanocubes is twice as much as that from Au nanocubes.[37] Therefore, while Au nanoparticles are often chosen because of their chemical stability to various surrounding environments, Ag nanoparticles are also chosen because of their higher RI susceptibilities.

Pd is a very attractive metal species, because it has various high-functionalities such as catalytic activity for many chemical reactions[38,39] and hydrogen storage capability.[40] Some Au-core/Pd-shell nanoparticles have recently been reported to exhibit high RI susceptibilities compared with unshelled Au nanoparticles.[15,41,42] All conventional interpretations of the enhanced susceptibility have centered on the plasmonic resonance of Au cores being perturbed by the presence of the Pd shell. Chen *et al.* reported enhanced RI susceptibility of Au nanorod-core/Pd-shell with discontinuous thin Pd shells, as compared with unshelled Au nanorods.[41] The enhancement was ascribed to the expulsion of the electric fields from Au nanorod cores by the adsorbed Pd shells. Zhang *et al.* reported that Au nanorods coated with Pd thin layers (thickness, ~1.1 nm) show a higher RI susceptibility than unshelled Au nanorods.[42] They suggested that the susceptibility enhancement originates from the red-shifted Au LSPR on the basis that the enhancement of the RI susceptibility of nanoparticles varies linearly with the LSPR wavelength.[43] Au-core/Pd-shell nanoparticles with thick Pd layers with a thickness of several tens of nanometers have recently been used to monitor the hydrogen adsorption on the Pd shell.[15] In this case, Au cores were assumed to act as plasmonic nanoantennae for detection of surface reactions. However, with such a thick Pd shell, the Pd LSPR should dominate while the Au LSPR is screened. Nevertheless, the intrinsic RI susceptibility of Pd LSPR itself has not yet been explicitly addressed.

In this study, we show that plasmonic Pd nanospheres (PdNSs) exhibit much higher susceptibility to RI changes than the commonly used nanoparticles such as Au nanospheres (AuNSs) and Ag nanospheres (AgNSs), both experimentally and theoretically. The results obtained in this study suggest that the Pd nanoparticle is a potential candidate for "the third plasmonic sensing material" following the typical Au and Ag toward the development of ultrahigh-sensitive LSPR sensors.

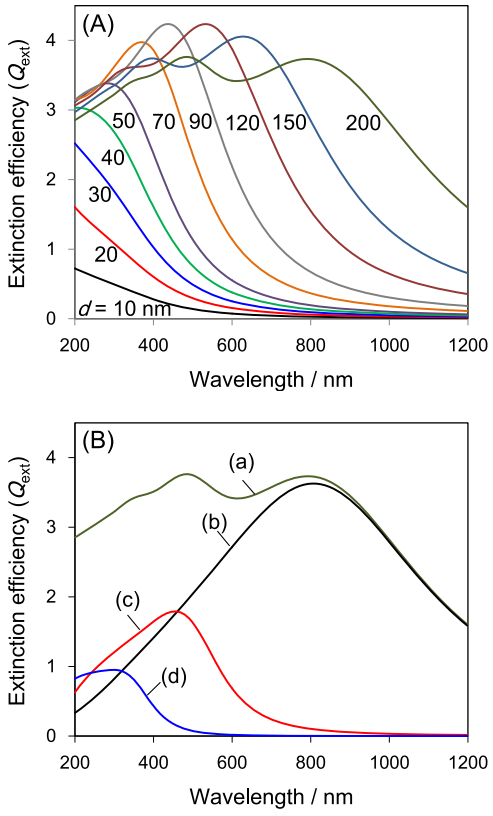

Figure 1. (A) Calculated extinction spectra of PdNSs in the range of d = 10−200 nm surrounded by water (n = 1.333) using Mie theory. Values on the curves indicate the assumed particle diameter (d). (B) Calculated extinction spectra of PdNSs 200 nm in diameter a. Curves b, c, and d represent the spectra obtained from the contribution of dipolar, quadrupolar, and octupolar LSPR modes, respectively.

RESULTS AND DISCUSSION

Overview of LSPR Properties of Pd Nanospheres (PdNSs). The LSPR properties of metal nanoparticles can be described by the Mie theory which gives analytical and exact solutions of the Maxwell equations for a classical, spherical nanoparticle with the multipolar expansion of the electromagnetic fields.[44] Here we describe the overview of the LSPR properties of PdNSs. Figure 1A shows the dependence of the extinction spectrum on the particle diameter (d) of PdNSs surrounded by water (n = 1.333) for a range of d = 10−200 nm simulated on the basis of the Mie theory. PdNSs smaller than 40 nm in diameter do not exhibit any LSPR peaks in the wavelength region longer than 200 nm. The larger PdNSs ($d \geq 50$ nm) show a single LSPR peak within the near-ultraviolet (UV) region, and those larger than 90 nm in diameter exhibit multiple, typically three, peaks within the range of 200−1200 nm. These three peaks can be attributed to dipolar, quadrupolar, and octupolar LSPR modes in order from the longer to shorter wavelength region

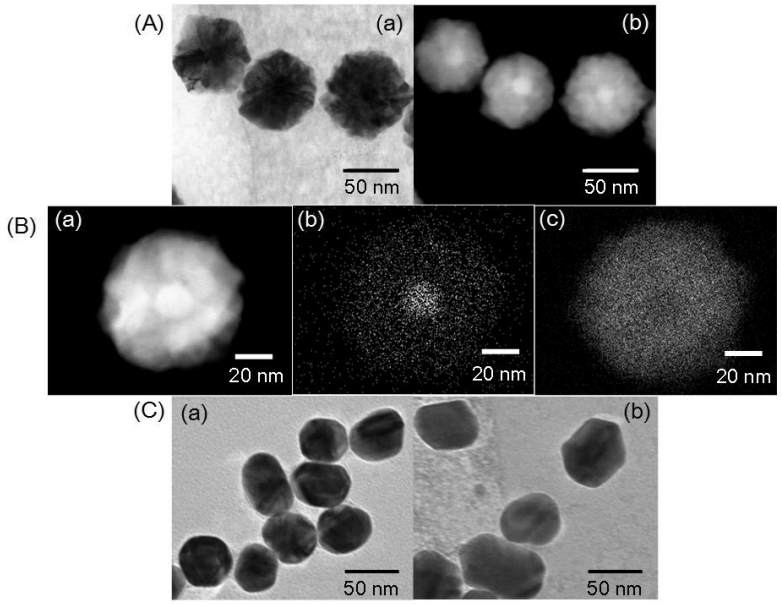

Figure 2. (A) Bright field (BF)-STEM image (a) and HAADF-STEM image (b) of Au/PdNSs. (B) HAADF-STEM image (a) and EDS elemental mapping of Au/PdNS; Au L edge (b) and Pd L edge (c). (C) TEM images of AuNSs (a) and AgNSs (b).

(Figure 1B). We notice that the band of the dipolar mode of PdNSs is much broader than those of AuNSs and AgNSs (see Figure S1 in Supporting Information) and it broadens further with shifting to a longer wavelength region. This is because the imaginary part of the dielectric function of Pd is larger than those of Au and Ag[45] and increases further with increasing wavelength because of an interband transition[46] (see Figure S2 in Supporting Information). Therefore, the use of PdNSs with 50−90 nm in diameter is best-suited for this work on the RI susceptibility to avoid excessive line-shape broadening. For PdNSs in this size range, the line shape is predominantly governed by the dipole mode, and overlapping with the other multipole peaks is minimal.

Morphological and Optical Characterization of Au/PdNSs. For the RI susceptibility of the LSPR of Pd nanoparticles to be properly evaluated in the frame of the Mie theory, we need to synthesize uniformly sized spherical Pd nanoparticles with the targeted diameter. However, it has been found that preparation of Pd nanoparticles consisting of pure Pd metallic species, particularly nanospheres, is quite difficult. Typical procedures include the use of polyvinylpyrrolidone (PVP)[47−49] or cetyltrimethylammonium bromide (CTAB)[50−54] as a bulky protective agent to disperse the particles in solution media. However, all of these attempts were ineffective and resulted in complicated geometries rather than a simple spherical shape. Further, the use of bulky protective agents to support the metal nanoparticles may end up with reductions of their susceptibility to RI changes.[23,37] Therefore, in this study, we adopted a seed-mediated growth method employing spherical Au nanoparticles as the seed cores. Applying an established method for the synthesis of Au-nanoparticle/Ag-shell,[55] we obtained highly reproducible spherical plasmonic Au nanoparticle-core/Pd-shell nanospheres (Au/PdNSs) protected with citric acid as a small capping molecules (full details are described in the Materials and Methods section).[56,57]

Formation of the Au/PdNSs was confirmed by high-angle annular dark-field scanning transmission electron microscope (HAADF-STEM) imaging and energy dispersive X-ray spectroscopy (EDS) mapping analysis. A HAADF-STEM image of the Au/PdNSs (panel b in Figure 2A) shows that the outer shell region was darker as compared with the core region. This is indicative of the presence of a high-Z element (Au) at the cores and a low-Z element (Pd) at the shells. Furthermore, EDS mapping images (Figure 2B) of the Au L edge and the Pd L edge ensured that Pd shells cover the whole surface of the Au cores.

The particle diameter of the Au/PdNSs of 73 ± 4 nm with the Au core diameter of 20 ± 1 nm was found by analyzing the TEM images of the particles by the ImageJ software (the TEM image of the Au cores is shown in Figure S3 in the Supporting Information).[58] Therefore, the thickness of Pd shells was estimated to be 27 ± 2 nm.

For comparison purposes, we also synthesized commonly used plasmonic spherical nanoparticles (AuNSs and AgNSs) protected with the same capping molecule (citric acid) (full details of the syntheses are described in the Materials and Methods section). The particle diameters of 60 ± 3 nm for AuNSs, 70 ± 4 nm for AgNSs, estimated from TEM observation (Figure 2C) were similar to that of Au/PdNS. The TEM images with low magnification for all of the nanospheres are shown in Supporting Information, Figure S4.

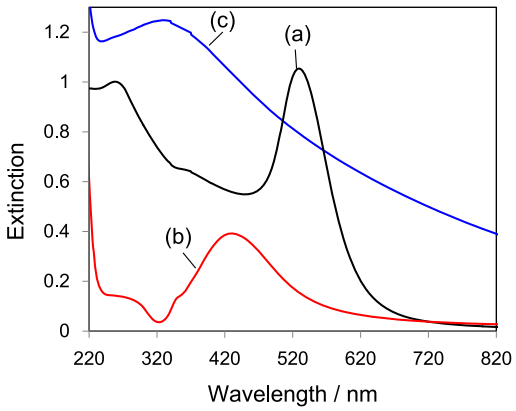

Figure 3. Extinction spectra of colloidal aqueous solutions of AuNSs (a), AgNSs (b), and Au/PdNSs (c).

The extinction spectra for the colloidal aqueous solutions of AuNSs, AgNSs, and Au/PdNSs are shown in Figure 3. Each of the solutions of AuNSs and AgNSs showed a sharp LSPR peak, which is attributable to the dipole resonance mode (535 nm for AuNSs and 440 nm for AgNSs). In addition, AgNSs showed a weak shoulder originating from the quadrupole resonance at approximately 350 nm. On the other hand, the solution of Au/PdNSs showed a clear broad extinction peak at 336 nm. To clarify the optical properties, the theoretical spectra of Au/PdNSs with a particle diameter of 73 nm with the Pd shell of 27 nm thickness were calculated from the Mie theory. The results are shown in Figure 4A: Curve a is the contribution of only the dipole resonance while curve b is the overall spectrum including the multipole resonances in addition to the dipole resonance. The experimentally obtained spectrum (curve c in Figure 4A) is in excellent agreement with the calculated spectra. Furthermore, these calculated spectra indicate that the LSPR peak from the Au/PdNSs in the measured wavelength range arises predominantly from the dipole resonance with only a small additional contribution of higher-order multipole resonances (e.g., quadrupole resonance).

As we are interested in the LSPR from the Pd nanosphere, we have investigated the effect of the Au cores on the LSPR properties of the Au/PdNSs. Figure 4B shows theoretical extinction spectra in water for Au/PdNSs having the total diameter of 73 nm with various diameters of Au-core. The Au/PdNSs with larger core diameters over 40 nm give the core/shell mode originating from the Au core in a 500−600 nm region in addition to a broad extinction peak of PdNSs covering the whole visible range. On the other hand, the spectra of the Au/PdNSs with the Au core diameters smaller than 30 nm showed only a broad LSPR peak, which is attributable to PdNSs. The LSPR peak originated from Au cores was not observed because of the screening effect due to the thick Pd shells. As a result, the shapes of the extinction spectra of these nanospheres were identical to that of the pure PdNSs (d = 0 nm in

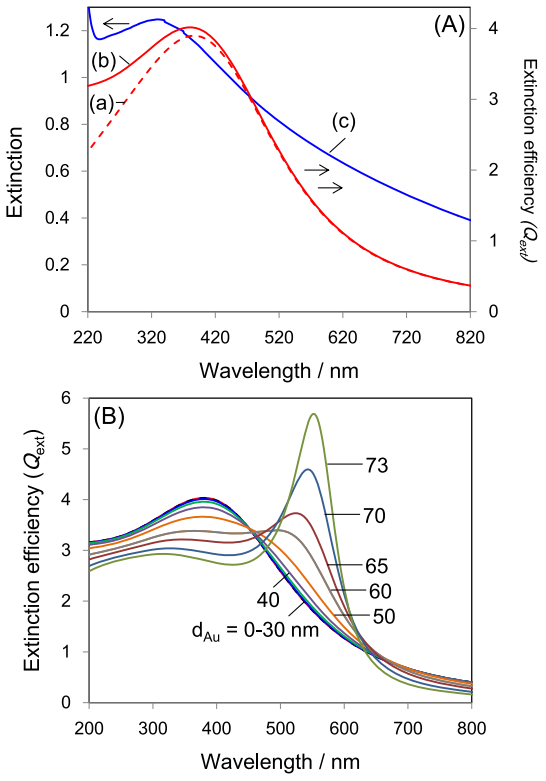

Figure 4. (A) Calculated extinction spectra of Au/PdNSs with the same morphology as experimentally obtained nanoparticles, surrounded by water (n = 1.333) consisting of only dipolar (a) and multipolar LSPR modes (b). Experimental extinction spectrum of colloidal aqueous solution of Au/PdNSs (c) (the same as in Figure 3c). (B) Au core size dependence of the calculated extinction spectra of Au/PdNSs (total diameter, 73 nm) within the region of 0−73 nm in the core diameters; d_{Au} values in the figure indicate the assumed Au core sizes.

Figure 4B). The experimentally obtained extinction spectrum for the Au/PdNSs with the 20 nm core diameter, which is consistent with the calculated spectra for Au/PdNSs with the core diameters smaller than 30 nm, is therefore attributable to the LSPR from the PdNSs, and the effect of the Au core is negligible. These results allow us to evaluate the intrinsic RI susceptibility of Pd using the present Au/PdNSs without the interference from the sufficiently small Au core.

Response to Refractive Index Changes. To investigate the optical response to the surrounding medium RI changes for the Au/PdNSs, we have immobilized Au/PdNSs on a quartz substrate. We also prepared AuNSs- and AgNSs-immobilized samples as the references. Typically, immersion of polyethylenimine (PEI)-modified quartz substrate in the colloidal aqueous solutions of the nanoparticles for appropriate duration led to the formation of well-dispersed nanoparticle assemblies *via* electrostatic interaction between the positively-charged quartz surface modifier and the negatively-charged nanoparticle surfaces, which are derived from citric acid used as a capping molecule. The extinction spectra of the nanospheres were measured in water

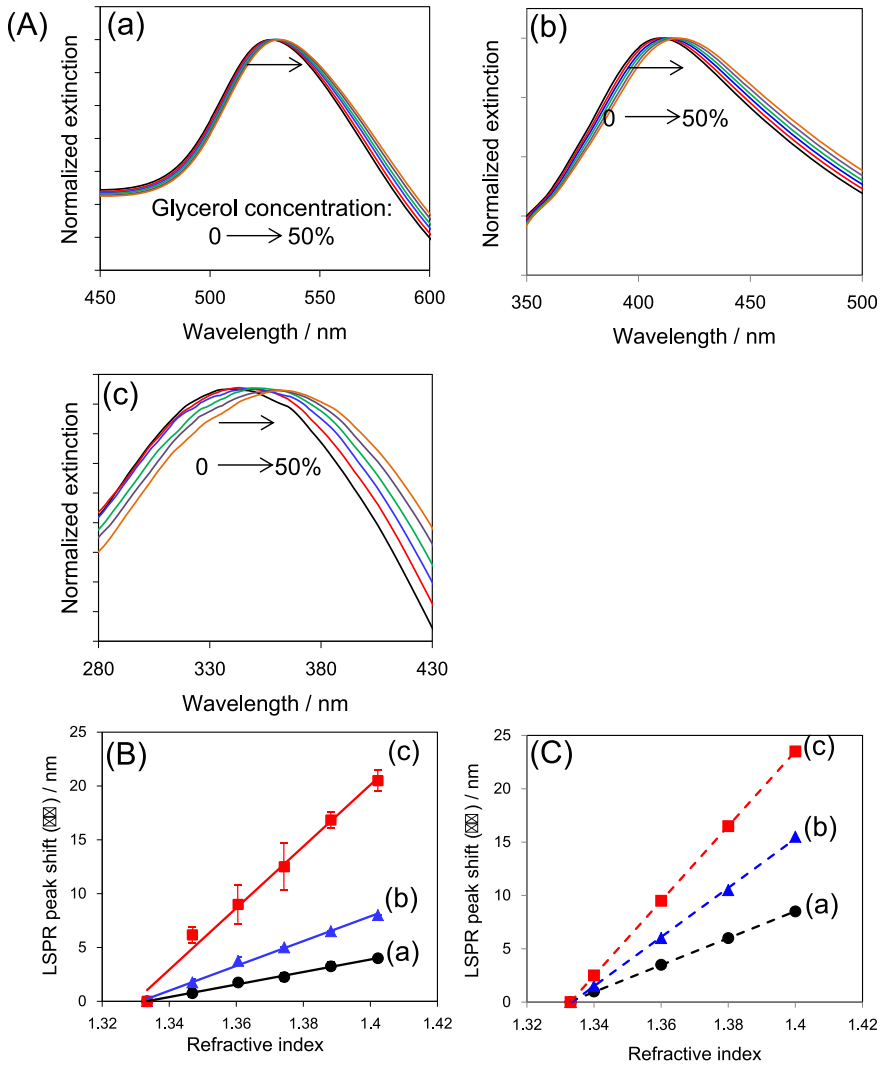

Figure 5. (A) Extinction spectra of the quartz substrate-supported AuNSs (a), AgNSs (b), and Au/PdNSs (c) in different solvent mixtures (0, 10, 20, 30, 40, and 50 vol % glycerol aqueous solutions). To highlight the spectral shift, all of the spectra are normalized. (B) Experimentally obtained dependences of the LSPR peak shifts on RI changes for AuNSs (a), AgNSs(b), and Au/PdNSs(c). (C) Calculated dependences of the LSPR peak shifts on RI changes for AuNSs (a), AgNSs(b), and PdNSs(c) with the same morphology as experimentally obtained nanoparticles.

(glycerol concentration: 0 vol %) and aqueous solutions of glycerol (10, 20, 30, 40, and 50 vol %). The refractive indexes (n_{bulk}) of the glycerol aqueous solutions were calculated according to the Lorentz−Lorenz equation.[22] The extinction spectrum for each of the immobilized nanospheres showed only LSPR modes originated from isolated nanoparticles but no coupling modes from multiple nanosphere aggregates (see Figure S5 in the Supporting Information). The absence of nanosphere aggregation was supported by the SEM images of AuNSs, AgNSs, and Au/PdNSs immobilized on the substrates; one can observe that the nanospheres were mostly monodispersed (Supporting Information Figure S6), with deposition densities of 6.5 ± 1.6 particles/μm^2 for AuNSs, 9.2 ± 2.3 for AgNSs, and 8.5 ± 0.8 for Au/PdNSs. Figure 5A shows the normalized extinction spectra (AuNSs (a), AgNSs (b), and Au/PdNSs (c)) for the immobilized nanoparticles in these solutions. All the LSPR peaks of the nanospheres red-shifted upon increasing the glycerol concentration, hence upon increasing the RI of the surrounding medium. As shown in Figure 5B, the LSPR peak shifts, $\Delta\lambda_{max}$ = (λ_{max} in glycerol solution) − (λ_{max} in water), for all three nanoparticles were linear to the changes in the RI of the surrounding medium ranging from 1.333 to 1.402. The RI susceptibility, defined as $S_{exp} = \Delta\lambda_{max}/\Delta n_{bulk}$, where Δn_{bulk} = (n_{bulk} in glycerol solution) − (n_{bulk} in water), of the nanospheres obtained from the linear fitting of the LSPR shifts versus the RI changes are shown in Table 1. The RI susceptibility of the AgNSs and AuNSs are consistent with previous reports.[4,59,60] The value of AgNSs is higher than that of AuNSs.[36,37] The new finding in the present study is that the RI susceptibility of Au/PdNSs is much higher than those of the AuNSs (4.9 times) and AgNSs (2.5 times).

We calculated RI susceptibilities from the LSPR peak shifts of AuNSs, AgNSs, and Au/PdNSs surrounded by

TABLE 1. Comparison of RI Susceptibility of AuNSs, AgNSs, Au/PdNSs, and PdNSs Obtained from Experimental Results (S_{exp}), Mie Theory (S_{Mie}), and QS Approximation (S_{QS})

	RI susceptibility (nm/RU)		
nanospheres	S_{exp}	S_{Mie}	S_{QS}
AuNSs	58 ± 0	126	134
AgNSs	115 ± 2	230	199
Au/PdNSs	286 ± 17		
PdNSs		351	290

media whose RI range is 1.333−1.400 using the Mie exact solution. As shown in Figure 5C, theoretically estimated RI susceptibilities (S_{Mie}) of these nanoparticles well reproduced the order of the experimentally obtained results (Figure 5B). The theoretical S_{Mie} of PdNSs is indeed quite high as shown in Table 1. These S_{Mie} values were calculated for nanospheres with experimentally obtained diameters in this study (AuNSs, 60 nm; AgNSs, 70 nm; and Au/PdNSs, 73 nm). The same trend is also obtained for nanospheres with an identical diameter (see Supporting Information, Table S1). The experimentally obtained RI susceptibilities are somewhat smaller than the theoretical ones because the susceptibilities were measured for nanoparticles immobilized on a quartz substrate surface whose RI is fixed, resulting in reduced overall susceptibility to the RI changes in the bulk solution, which is called the "substrate effect".[61]

Origin of High RI Susceptibility of Pd LSPR. Although the Mie theory predicts the high susceptibility of Au/PdNSs as described above, it is difficult to extract physically meaningful factors from the full formulation of the theory. Therefore, we have examined the factors determining the high susceptibility of plasmonic Pd nanoparticles using a perturbation theory. Specifically, the ratio (S_{QS}) of a small change of the LSPR wavelength, $\Delta\lambda$, to a small change of RI, Δn, can be described in a quasi-static (QS) approximation framework as follows.[43]

$$S_{QS} = \frac{\Delta\lambda}{\Delta n} = \frac{2\varepsilon_1}{n}\left(\left.\frac{\partial\varepsilon_1}{\partial\lambda}\right|_{\lambda_0}\right)^{-1} \quad (1)$$

where ε_1, n, λ, and λ_0, are, respectively, the real part of the dielectric function of the metal, the refractive index of the medium, the wavelength of incident light, and the LSPR peak wavelength. This equation tells us that the high susceptibility of the Au/PdNSs originates either from a large value of ε_1 or a small dispersion of ε_1 at the resonant wavelength or both. Under the QS approximation, the extinction cross-section (σ_{ext}) of the metal nanospheres is described as[44]

$$\sigma_{ext} = \frac{24\pi^2 n^3 a^3}{\lambda}\cdot\frac{\varepsilon_2}{(\varepsilon_1+2n^2)^2+\varepsilon_2{}^2} \quad (2)$$

where a is the radius of metal nanosphere and ε_2 is the imaginary part of the dielectric function of the metal.

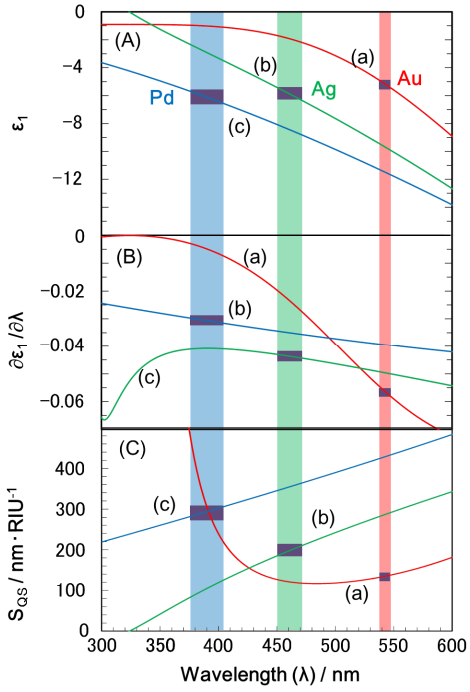

Figure 6. (A) Wavelength dependences of real part of the dielectric functions (ε_1) of Au (a), Ag (b), and Pd (c). (B) Dispersion of ε_1 ($\partial\varepsilon_1/\partial\lambda$) of Au, Ag, and Pd. (C) RI susceptibility (S_{QS}) of Au, Ag, Pd. The vertical column of each color means the LSPR region for the RI from n = 1.333 to 1.400. The width of the column corresponds to the susceptibility. Purple marks indicate the value of each property, ε_1, $\partial\varepsilon_1/\partial\lambda$, and S_{QS} in the resonance wavelength range.

The LSPR peak position corresponds to the wavelength where σ_{ext} takes the maximum value. It is well-known that σ_{ext} takes the maximum at the wavelength at which the Fröhlich condition $\varepsilon_1 + 2n^2 = 0$ is satisfied in the dipolar LSPR mode in many metal nanospheres including Au, Ag, and Pd, because the dispersion of ε_2 is smaller than that of ε_1 around the resonant wavelength for these metals. Therefore, the value of ε_1 that satisfies the resonant condition is determined by the medium and would not depend on the kind of metals. In Figure 6(A), ε_1 is plotted against wavelength for each metallic species (ε_1 values for Au, Ag, and Pd were taken from ref 45. 62, and46, respectively.). Also shown in Figure 6 are the vertical shaded columns that indicate the ranges of LSPR peak positions in solvents from water to 50 vol % glycerol/water calculated by the Mie theory. The purple rectangles indicating the crossing regions then represent the ε_1 values at the resonant conditions for Pd, Ag, and Au. We see that the values of ε_1 at the resonant conditions for each metal species are close to one another (ε_1 = −5.19 for Au around 543 nm, −6.10 for Ag around 466 nm, and −6.20 for Pd around 393 nm for n_{bulk} = 1.37: average value of refractive indices of water and 50 vol % glycerol/water). Note that the Fröhlich condition can be applied for spheres much smaller than the wavelength. The obtained ε_1 values for resonance are somewhat different from that (ε_1 = −3.75 for n_{bulk} = 1.37)

calculated according to the Fröhlich condition, because the size parameter has to be taken into account and because the Fröhlich condition should be modified for spherical larger nanoparticles. However, even if the size parameters are taken into account, values of ε_1 for each metal species are close to one another (see Supporting Information). Therefore, the difference in the RI susceptibility is determined not by the difference in ε_1 but mainly by the difference in the dispersion of ε_1, that is, $\partial\varepsilon_1/\partial\lambda$. Figure 6 parts B and C show, respectively, the $\partial\varepsilon_1/\partial\lambda$ values and the RI susceptibility (S_{QS}) at the resonant wavelengths obtained from eq 1. Clearly, smaller $|\partial\varepsilon_1/\partial\lambda|$ values lead to larger S_{QS} values for Au (134 nm·RIU^{-1}), Ag (199 nm·RIU^{-1}), and Pd (290 nm·RIU^{-1}) at the respective resonant wavelengths. These theoretical RI susceptibilities are well in agreement with the susceptibilities (S_{Mie}) obtained by the full Mie theory taking all multipole expansions into considerations (see Table 1). While application of the QS approximation is regarded to be valid for the metal nanoparticles with diameters much smaller than the wavelength of light and with a sufficiently small real part of the dielectric function, the above discussions clearly demonstrate the validity of the QS approximation in the present case, although the sizes of the metal nanoparticles are relatively large.[63] Taken together, the origin of the large RI susceptibility of the Pd plasmonic nanoparticles is attributed to the small dispersion of the real part of the dielectric function at the LSPR wavelength ($\partial\varepsilon_1/\partial\lambda$).

Although we have made a thorough literature survey of the RI susceptibility of Pd LSPR, we found no report demonstrating either theoretically or experimentally that RI susceptibility of Pd LSPR is much higher than those of the commonly used plasmonic metals (Au and Ag). This might be due to synthetic difficulty of uniformly sized spherical Pd nanoparticles with the targeted diameter and/or handling difficulty of the Pd nanoparticles. For example, air exposure and drying of Pd nanoparticles with a diameter of several tens of nanometers causes irreversible damping of the LSPR as we have often experienced. In the present work, we succeeded in the synthesis of the targeted diameter by employing the seed-mediated growth method. We further made it possible to maintain the intrinsic RI susceptibility of Pd LSPR by preventing the Au/PdNSs on the substrates in solution from drying. To our delight, we found that the susceptibility of Au/PdNSs is truly higher than those of some previously reported anisotropic nanoparticles consisting of the commonly used plasmonic Au species such as Au nanorods (198−288 nm RIU^{-1}),[22−24] Au nanopyramids (130−221 nm RIU^{-1}),[26] Au nanocubes (83 and 147 nm RIU^{-1}),[22,37] Au nanobars (219 nm RIU^{-1}),[37] and Au nanotube arrays (250 nm RIU^{-1}),[64] although higher susceptibility values have been reported for Au nanoparticles with complex geometries such as Au nanostars (660 nm RIU^{-1}),[25] Au nanobranches (703 nm RIU^{-1}),[22] Au nanoprisms (737 nm RIU^{-1}),[28] Au nanorings (880 nm RIU^{-1}),[33] and Au nanoframes (740 nm RIU^{-1}).[32] The synthetic processes of these anisotropic sensing nanoparticles are mostly quite complex and time-consuming, as compared with those of simple spherical nanoparticles employed in the present study. Also, synthesis of many of these anisotropic nanoparticles requires dense and bulky protective coating with molecules such as polyvinylpyrrolidone (PVP)[31,32,37] and cetyltrimetylammonium bromide (CTAB),[22,25,27,28] which may prevent the receptor molecules such as antibodies, which will be required for application to biosensors, from gaining access to the close proximity to the metal. In contrast, the spherical nanoparticles can be synthesized utilizing small molecules such as citric acid as a capping molecule. It has recently been reported that Pd surfaces are very active for surface immobilization of self-assembled monolayers based on sulfur-Pd bonding.[65,66] Therefore, these results suggest that the Au/PdNSs can act as plasmonic sensing materials with a superior sensitivity, an easier synthesis, and more facile surface modification with functional molecules, than conventional Au- and Ag-based nanoparticles.

Although Au/PdNSs has the large RI susceptibility, their LSPR signals are broad due to the large imaginary part of the dielectric function. The sensitivity of the LSPR sensors is mainly determined by the figure of merit (FoM), which is defined as the ratio of the RI susceptibility to the resonance width. Therefore, the broader LSPR peak might be considered as detrimental to the sensing based on RI changes because this is directly linked to a lower FoM. However, this disadvantage can be potentially resolved by the following two approaches.

First, the peak positions can be read out only from the LSPR spectrum itself but also from the second derivative (curvature) of the spectrum. It is theoretically possible that the latter monitoring method will resolve the disadvantage of broad LSPR.[67]

Second, one of the attractive phenomena that are deemed useful for the development of highly sensitive LSPR sensors is the Fano resonance which occurs in metallic complex nanostructures because it can enhance the FoM due to their sharp lineshapes.[68] This unique phenomenon has been studied in heterogeneous nanostructures consisting of Au−Pd,[69] and Ag−Pd[70] as well as the aggregated nanostructures consisting of the monometals. The Fano resonances generated from the heterostructures consisting of Pd and other metals have a great potential for highly sensitive sensors.

CONCLUSIONS

This study demonstrated that the Pd nanoparticle is a promising candidate for "the third plasmonic sensing material" to be used in ultrahigh-sensitive LSPR sensors. We experimentally and theoretically demonstrated that

the RI susceptibility of the Pd LSPR peak from Au/PdNSs, which is attributable to a dipole mode, is much higher than commonly used plasmonic sensing nanospheres (AuNSs and AgNSs). In addition, we found using the QS approximation that this high susceptibility arises from the small dispersion of the real part of the dielectric function of the metal. These results demonstrated that the Pd LSPR has a high degree of usability as a sensing mechanism for label-free biosensing, gas sensing, and so on. Furthermore, we proposed that the monitoring of the curvature of LSPR signal and the Fano resonance, which occur in heterostructures consisting of the Pd−Au(Ag), will lead to an improved FoM.

MATERIALS AND METHODS

Chemicals. Milli-Q-grade water was used to prepare up all aqueous solutions. Palladium(II) chloride ($PdCl_2$; Wako Pure Chemicals), 0.2 M hydrochloric acid (HCl; Wako Pure Chemicals), trisodium citrate dihydrate (Kanto Chemical), L-ascorbic acid (Wako Pure Chemicals), hydrogen tetrachloroaurate(III) tetrahydrate ($HAuCl_4 \cdot 4H_2O$; Nacalai Tesque), silver nitrate ($AgNO_3$; Wako Pure Chemicals), poly(ethylenimine) (PEI, M_w = 50 000−100 000; Wako Pure Chemicals), poly(sodium 4-styrenesulfonate) (PSS, M_w = 70 000; Sigma-Aldrich), and glycerol (Sigma-Aldrich) were used as purchased without further purification.

Preparation of Colloidal Aqueous Solution of Au/PdNSs. A colloidal aqueous solution of gold nanoparticle cores was prepared using a modified version of previously reported procedures.[71] Typically, an aqueous solution of $HAuCl_4 \cdot 4H_2O$ (0.01 wt %, 100 mL) was refluxed for 30 min. Next, an aqueous solution of trisodium citrate (1 wt %, 4 mL) was added instantaneously into the solution, followed by refluxing for 60 min to produce an aqueous solution of gold nanoparticles (mean diameter: 20 ± 1 nm) protected with citric acids. Then, an aqueous solution of hydrogen tetrachloropalladate(II) (1 mM, H_2PdCl_4) was prepared by dissolving 1.7 mg of $PdCl_2$ into 10 mL of a 1 mM HCl aqueous solution. Next, 0.6 mL of the solution of gold nanoparticle cores was added to the H_2PdCl_4 solution, and 1.2 mL of an aqueous solution of ascorbic acid (100 mM) was added to the solution at a speed of 8 μL per minute in an ice bath.[56] The color of the solution gradually turned to dark brown. The stirring was continued for 30 min after finishing the addition of ascorbic acid solution. Finally, the resultant colloidal solution was centrifuged for 15 min at 14 000 rpm, followed by dispersing the obtained precipitations of Au/PdNSs into an aqueous solution of trisodium citrate (1.3 mM, 10 mL).

Preparation of Colloidal Aqueous Solutions of AuNSs and AgNSs. A colloidal aqueous solution of AuNSs was prepared using a modified version of the above-described procedures.[71] Typically, an aqueous solution of $HAuCl_4 \cdot 4H_2O$ (0.01 wt %, 50 mL) was refluxed for 30 min. Next, an aqueous solution of disodium citrate (1 wt %, 0.45 mL) was injected into the solution and then the mixed solution was refluxed for 60 min to produce an aqueous solution of citrate-capped AuNSs (diameter, 60 ± 3 nm). A colloidal aqueous solution of AgNSs (diameter, 70 ± 4 nm) protected with citric acid was prepared using Meisel's procedure.[72] An aqueous solution of silver nitrate (1 mM, 100 mL) was refluxed for 30 min. Then, a 2 mL aliquot of aqueous sodium citrate (10 wt %) was added to the solution, and the solution was again refluxed for 1 h.

Immobilization of Metal Nanoparticles. To investigate RI susceptibilities of the plasmonic nanoparticle, the nanoparticles were immobilized on the surface of a quartz substrate. First, the substrate was immersed into an aqueous solution of PEI (45 mg/mL) containing 0.2 M NaCl for 30 min at room temperature. After washing the surface with water, the substrate was immersed into an aqueous solution of PSS (42 mg/mL) containing 0.2 M NaCl for 30 min at room temperature. Next, after washing the surface with water, the surface was again immersed into the PEI solution, followed by washing with water. The substrate covered with the resultant positively charged surface layer was then immersed into colloidal aqueous solutions of each of the metal nanoparticles for appropriate duration (AuNSs and AgNSs for 3 h and Au/PdNSs for 12 h), followed by washing with water.[73] All of the aqueous solutions for immobilization of the nanospheres were used without degassing. On the other hand, the nanospheres immobilized on the substrates were kept away from direct exposure to gaseous air to avoid deterioration of the nanospheres.

Measurements and Calculations. UV−vis spectral measurements were carried out by a JASCO V-630 spectrophotometer. TEM images were taken on a Hitachi HF-2000 with an acceleration voltage of 200 kV. A HAADF-STEM image and EDS mapping analysis were taken on a STEM (HD-2300C, Hitachi Ltd.). FE-SEM images were taken with a Hitachi S-4500 microscope with an acceleration voltage of 15 kV. Mie scattering calculation was carried out by Bohren and Huffman's solution[42] using the MATLAB code written by Mätzler.[74] Dielectric functions for the metals was taken from the 4-term Lorentzian model for Au,[45] the Drude−Lorentz model for Ag,[62] and the Drude model for Pd.[46]

Conflict of Interest: The authors declare no competing financial interest.

Acknowledgment. This work was supported in part by Grant-in-Aid for Young Scientists B (Grant No. 26810102) from JSPS KAKENHI.

Supporting Information Available: Calculated extinction spectra of AuNSs and AgNSs (Figure S1), wavelength dependences of imaginary part of the dielectric functions (ε_2) of Au, Ag, and Pd (Figure S2), TEM image of Au cores (Figure S3), TEM images with low magnification of AuNSs, AgNSs, and Au/PdNSs (Figure S4), extinction spectra in water for AuNSs, AgNSs, and Au/PdNSs-immobilized quartz (Figure S5), SEM images of AuNSs, AgNSs, and Au/PdNSs immobilized on quartz substrates (Figure S6), RI susceptibility of AuNSs, AgNSs, and Au/PdNSs obtained from the Mie theory (S_{Mie}) (Table S1) and discussion about resonant condition of localized surface plasmon for a large nanoparticle are given. This material is available free of charge *via* the Internet at http://pubs.acs.org.

REFERENCES AND NOTES

1. Giannini, V.; Fernández-Domínguez, A. I.; Heck, S. C.; Maier, S. A. Plasmonic Nanoantennas: Fundamentals and Their Use in Controlling the Radiative Properties of Nanoemitters. *Chem. Rev.* **2011**, *111*, 3888–3912.
2. Underwood, S.; Mulvaney, P. Effect of the Solution Refractive Index on the Color of Gold Colloids. *Langmuir* **1994**, *10*, 3427–3430.
3. Anker, J. N.; Hall, W. P.; Lyandres, O.; Shah, N. C.; Zhao, J.; Van Duyne, R. P. Biosensing with Plasmonic Nanosensors. *Nat. Mater.* **2008**, *7*, 442–453.
4. Mayer, K. M.; Hafner, J. H. Localized Surface Plasmon Resonance Sensors. *Chem. Rev.* **2011**, *111*, 3828–3857.
5. Mayer, K. M.; Lee, S.; Liao, H.; Rostro, B. C.; Fuentes, A.; Scully, P. T.; Nehl, C. L.; Hafner, J. H. A Label-Free Immunoassay Based Upon Localized Surface Plasmon Resonance of Gold Nanorods. *ACS Nano* **2008**, *2*, 687–692.
6. Tian, L.; Morrissey, J. J.; Kattumenu, R.; Gandra, N.; Kharasch, E. D.; Singamaneni, S. Bioplasmonic Paper as a Platform for Detection of Kidney Cancer Biomarkers. *Anal. Chem.* **2012**, *84*, 9928–9934.
7. Chang, Y.-F.; Hung, S.-H.; Lee, Y.-J.; Chen, R.-C.; Su, L.-C.; Lai, C.-S.; Chou, C. Discrimination of Breast Cancer by Measuring Prostate-Specific Antigen Levels in Women's Serum. *Anal. Chem.* **2011**, *83*, 5324–5328.

8. Truong, P. L.; Kim, B. W.; Sim, S. J. Rational Aspect Ratio and Suitable Antibody Coverage of Gold Nanorod for Ultra-Sensitive Detection of a Cancer Biomarker. *Lab. Chip* **2012**, *12*, 1102–1109.
9. Sönnichsen, C.; Reinhard, B. M.; Liphardt, J.; Alivisatos, A. P. A Molecular Ruler Based on Plasmon Coupling of Single Gold and Silver Nanoparticles. *Nat. Biotechnol.* **2005**, *23*, 741–745.
10. Sannomiya, T.; Hafner, C.; Voros, J. *In Situ* Sensing of Single Binding Events by Localized Surface Plasmon Resonance. *Nano Lett.* **2008**, *8*, 3450–3455.
11. Bingham, J. M.; Anker, J. N.; Kreno, L. E.; Van Duyne, R. P. Gas Sensing with High-Resolution Localized Surface Plasmon Resonance Spectroscopy. *J. Am. Chem. Soc.* **2010**, *132*, 17358–17359.
12. Kreno, L. E.; Hupp, J. T.; Van Duyne, R. P. Metal–Organic Framework Thin Film for Enhanced Localized Surface Plasmon Resonance Gas Sensing. *Anal. Chem.* **2010**, *82*, 8042–8046.
13. Larsson, E. M.; Langhammer, C.; Zorić, I.; Kasemo, B. Nanoplasmonic Probes of Catalytic Reactions. *Science* **2009**, *326*, 1091–1094.
14. Liu, N.; Tang, M. L.; Hentschel, M.; Giessen, H.; Alivisatos, A. P. Nanoantenna-Enhanced Gas Sensing in a Single Tailored Nanofocus. *Nat. Mater.* **2011**, *10*, 631–636.
15. Chiu, C.-Y.; Huang, M. H. Polyhedral Au–Pd Core–Shell Nanocrystals as Highly Spectrally Responsive and Reusable Hydrogen Sensors in Aqueous Solution. *Angew. Chem., Int. Ed.* **2013**, *52*, 12709–12713.
16. Langhammer, C.; Larsson, E. M.; Kasemo, B.; Zorić, I. Indirect Nanoplasmonic Sensing: Ultrasensitive Experimental Platform for Nanomaterials Science and Optical Nanocalorimetry. *Nano Lett.* **2010**, *10*, 3529–3538.
17. Langhammer, C.; Zorić, I.; Kasemo, B. Hydrogen Storage in Pd Nanodisks Characterized with a Novel Nanoplasmonic Sensing Scheme. *Nano Lett.* **2007**, *7*, 3122–3127.
18. Tang, M. L.; Liu, N.; Dionne, J. A.; Alivisatos, A. P. Observations of Shape-Dependent Hydrogen Uptake Trajectories from Single Nanocrystals. *J. Am. Chem. Soc.* **2011**, *133*, 13220–13223.
19. Wang, F.; Sun, L.-D.; Feng, W.; Chen, H.; Yeung, M. H.; Wang, J.; Yan, C.-H. Heteroepitaxial Growth of Core–Shell and Core–Multishell Nanocrystals Composed of Palladium and Gold. *Small* **2010**, *6*, 2566–2575.
20. Jiang, R.; Qin, F.; Ruan, Q.; Wang, J.; Jin, C. Ultrasensitive Plasmonic Response of Bimetallic Au/Pd Nanostructures to Hydrogen. *Adv. Funct. Mater.* **2014**, *24*, 7328–7337.
21. Nath, N.; Chilkoti, A. Label-Free Biosensing by Surface Plasmon Resonance of Nanoparticles on Glass: Optimization of Nanoparticle Size. *Anal. Chem.* **2004**, *76*, 5370–5378.
22. Chen, H.; Kou, X.; Yang, Z.; Ni, W.; Wang, J. Shape- and Size-Dependent Refractive Index Sensitivity of Gold Nanoparticles. *Langmuir* **2008**, *24*, 5233–5237.
23. Omura, N.; Uechi, I.; Yamada, S. Comparison of Plasmonic Sensing between Polymer- and Silica-Coated Gold Nanorods. *Anal. Sci.* **2009**, *25*, 255–259.
24. Jain, P. K.; Huang, X.; El-Sayed, I. H.; El-Sayed, M. A. Noble Metals on the Nanoscale: Optical and Photothermal Properties and Some Applications in Imaging, Sensing, Biology, and Medicine. *Acc. Chem. Res.* **2008**, *41*, 1578–1586.
25. Nehl, C. L.; Liao, H.; Hafner, J. H. Optical Properties of Star-Shaped Gold Nanoparticles. *Nano Lett.* **2006**, *6*, 683–688.
26. Lee, J.; Hasan, W.; Odom, T. W. Tuning the Thickness and Orientation of Single Au Pyramids for Improved Refractive Index Sensitivities. *J. Phys. Chem. C* **2009**, *113*, 2205–2207.
27. Khalavka, Y.; Becker, J.; Sönnichsen, C. Synthesis of Rod-Shaped Gold Nanorattles with Improved Plasmon Sensitivity and Catalytic Activity. *J. Am. Chem. Soc.* **2009**, *131*, 1871–1875.
28. Banholzer, M. J.; Harris, N.; Millstone, J. E.; Schatz, G. C.; Mirkin, C. A. Abnormally Large Plasmonic Shifts in Silica-Protected Gold Triangular Nanoprisms. *J. Phys. Chem. C* **2010**, *114*, 7521–7526.
29. Charles, D. E.; Aherne, E.; Gara, M.; Ledwith, D. M.; Gun'ko, Y. K.; Kelly, J. M.; Blau, W. J.; Brennan-Fournet, M. E. Versatile Solution Phase Triangular Silver Nanoplates for Highly Sensitive Plasmon Resonance Sensing. *ACS Nano* **2010**, *4*, 55–64.
30. Haes, A. J.; Van Duyne, R. P. A Nanoscale Optical Biosensor: Sensitivity and Selectivity of an Approach Based on the Localized Surface Plasmon Resonance Spectroscopy of Triangular Silver Nanoparticles. *J. Am. Chem. Soc.* **2002**, *124*, 10596–10604.
31. Sherry, L. J.; Chang, S.-H.; Schatz, G. C.; Van Duyne, R. P. Localized Surface Plasmon Resonance Spectroscopy of Single Silver Nanocubes. *Nano Lett.* **2005**, *5*, 2034–2038.
32. Mahmoud, M. A.; El-Sayed, M. A. Gold Nanoframes: Very High Surface Plasmon Fields and Excellent Near-Infrared Sensors. *J. Am. Chem. Soc.* **2010**, *132*, 12704–12710.
33. Larsson, E. M.; Alegret, J.; Käll, M.; Sutherland, D. S. Sensing Characteristics of NIR Localized Surface Plasmon Resonances in Gold Nanorings for Application as Ultrasensitive Biosensors. *Nano Lett.* **2007**, *7*, 1256–1263.
34. DeSantis, C. J.; Skrabalak, S. E. Size-Controlled Synthesis of Au/Pd Octopods with High Refractive Index Sensitivity. *Langmuir* **2012**, *28*, 9055–9062.
35. Jain, P. K.; El-Sayed, M. A. Noble Metal Nanoparticle Pairs: Effect of Medium for Enhanced Nanosensing. *Nano Lett.* **2008**, *8*, 4347–4352.
36. Haes, A. J.; Zou, S.; Schatz, G. C.; Van Duyne, R. P. A Nanoscale Optical Biosensor: The Long Range Distance Dependence of the Localized Surface Plasmon Resonance of Noble Metal Nanoparticles. *J. Phys. Chem. B* **2004**, *108*, 109–116.
37. Lee, Y. H.; Chen, H.; Xu, Q.-H.; Wang, J. Refractive Index Sensitivities of Noble Metal Nanocrystals: The Effects of Multipolar Plasmon Resonances and the Metal Type. *J. Phys. Chem. C* **2011**, *115*, 7997–8004.
38. Hartings, M. Reactions Coupled to Palladium. *Nat. Chem.* **2012**, *4*, 764.
39. Seechurn, C. C. C. J.; Kitching, M. O.; Colacot, T. J.; Snieckus, V. Palladium-Catalyzed Cross-Coupling: A Historical Contextual Perspective to the 2010 Nobel Prize. *Angew. Chem., Int. Ed.* **2012**, *51*, 5062–5085.
40. Horinouchi, S.; Yamanoi, Y.; Yonezawa, T.; Mouri, T.; Nishihara, H. Hydrogen Storage Properties of Isocyanide-Stabilized Palladium Nanoparticles. *Langmuir* **2006**, *22*, 1880–1884.
41. Chen, H.; Wang, F.; Li, K.; Woo, K. C.; Jianfang, W.; Li, Q.; Sun, L.-D.; Zhang, X.; Lin, H.-Q.; Yan, C.-H. Plasmonic Percolation: Plasmon-Manifested Dielectric-to-Metal Transition. *ACS Nano* **2012**, *6*, 7162–7171.
42. Zhang, K.; Xiang, Y.; Wu, X.; Feng, L.; He, W.; Liu, J.; Zhou, W.; Xie, S. Enhanced Optical Responses of Au@Pd Core/Shell Nanobars. *Langmuir* **2009**, *25*, 1162–1168.
43. Miller, M. M.; Lazarides, A. A. Sensitivity of Metal Nanoparticle Surface Plasmon Resonance to the Dielectric Environment. *J. Phys. Chem. B* **2005**, *109*, 21556–21565.
44. Bohren, C. F.; Huffman, D. R. *Absorption and Scattering of Light by Small Particles*; Wiley VCH: New York, 1983.
45. Hao, F.; Nordlander, P. Efficient Dielectric Function for FDTD Simulation of the Optical Properties of Silver and Gold Nanoparticles. *Chem. Phys. Lett.* **2007**, *446*, 115–118.
46. Pakizeh, T.; Langhammer, C.; Zoric, I.; Apell, P.; Käll, M. Intrinsic Fano Interference of Localized Plasmons in Pd Nanoparticles. *Nano Lett.* **2009**, *9*, 882–886.
47. Xiong, Y.; Chen, J.; Wiley, B.; Xia, Y. Understanding the Role of Oxidative Etching in the Polyol Synthesis of Pd Nanoparticles with Uniform Shape and Size. *J. Am. Chem. Soc.* **2005**, *127*, 7332–7333.
48. Xiong, Y.; Cai, H.; Wiley, B. J.; Wang, J.; Kim, M. J.; Xia, Y. Synthesis and Mechanistic Study of Palladium Nanobars and Nanorods. *J. Am. Chem. Soc.* **2007**, *129*, 3665–3675.
49. Li, C.; Sato, R.; Kanehara, M.; Zeng, H.; Bando, Y.; Teranishi, T. Controllable Polyol Synthesis of Uniform Palladium Icosahedra: Effect of Twinned Structure on Deformation of Crystalline Lattices. *Angew. Chem., Int. Ed.* **2009**, *48*, 6883–6887.

50. Xiong, Y.; McLellan, J. M.; Yin, Y.; Xia, Y. Synthesis of Palladium Icosahedra with Twinned Structure by Blocking Oxidative Etching with Citric Acid or Citrate Ions. *Angew. Chem., Int. Ed.* **2007**, *46*, 804–808.
51. Berhault, G.; Bausach, M.; Bisson, L.; Becerra, L.; Thomazeau, C.; Uzio, D. Seed-Mediated Synthesis of Pd Nanocrystals: Factors Influencing a Kinetic- or Thermodynamic-Controlled Growth Regime. *J. Phys. Chem. C* **2007**, *111*, 5915–5925.
52. Lim, B.; Xiong, Y.; Xia, Y. A Water-Based Synthesis of Octahedral, Decahedral, and Icosahedral Pd Nanocrystals. *Angew. Chem., Int. Ed.* **2007**, *46*, 9279–9282.
53. Zhang, J.; Zhang, L.; Xie, S.; Kuang, Q.; Han, X.; Xie, Z.; Zheng, L. Synthesis of Concave Palladium Nanocubes with High-Index Surfaces and High Electrocatalytic Activities. *Chem.—Eur. J.* **2011**, *17*, 9915–9919.
54. Shuai, D.; McCalman, D. C.; Choe, J. K.; Shapley, J. R.; Schneider, W. F.; Werth, C. J. Structure Sensitivity Study of Waterborne Contaminant Hydrogenation Using Shape- and Size-Controlled Pd Nanoparticles. *ACS Catal.* **2013**, *3*, 453–463.
55. Jana, N. R. Silver Coated Gold Nanoparticles as New Surface Enhanced Raman Substrate at Low Analyte Concentration. *Analyst* **2003**, *128*, 954–956.
56. Hua, J.-W.; Zhang, Y.; Li, J.-F.; Liu, Z.; Ren, B.; Sun, S.-G.; Tian, Z.-Q.; Lian, T. Synthesis of Au@Pd Core−Shell Nanoparticles with Controllable Size and Their Application in Surface-Enhanced Raman Spectroscopy. *Chem. Phys. Lett.* **2005**, *408*, 354–359.
57. Lu, L.; Wang, H.; Xi, S.; Zhang, H. Improved Size Control of Large Palladium Nanoparticles by a Seeding Growth Method. *J. Mater. Chem.* **2002**, *12*, 156–158.
58. Schneider, C. A.; Rasband, W. S.; Eliceiri, K. W. NIH Image to ImageJ: 25 years of image analysis. *Nat. Methods* **2012**, *9*, 671–675.
59. Sun, Y.; Xia, Y. Increased Sensitivity of Surface Plasmon Resonance of Gold Nanoshells Compared to That of Gold Solid Colloids in Response to Environmental Changes. *Anal. Chem.* **2002**, *74*, 5297–5305.
60. Dong, P.; Lin, Y.; Deng, J.; Di, J. Ultrathin Gold-Shell Coated Silver Nanoparticles onto a Glass Platform for Improvement of Plasmonic Sensors. *ACS Appl. Mater. Interfaces* **2013**, *5*, 2392–2399.
61. Dmitriev, A.; Hägglund, C.; Chen, S.; Fredriksson, H.; Pakizeh, T.; Käll, M.; Sutherland, D. S. Enhanced Nanoplasmonic Optical Sensors with Reduced Substrate Effect. *Nano Lett.* **2008**, *8*, 3893–3898.
62. Rakić, A. D.; Djurišić, A. B.; Elazar, J. M.; Majewski, M. L. Optical Properties of Metallic Films for Vertical-Cavity Optoelectronic Devices. *Appl. Opt.* **1998**, *37*, 5271–5283.
63. Lee, K.-S.; El-Sayed, M. A. Gold and Silver Nanoparticles in Sensing and Imaging: Sensitivity of Plasmon Response to Size, Shape, and Metal Composition. *J. Phys. Chem. B* **2006**, *110*, 19220–19225.
64. McPhillips, J.; Murphy, A.; Jonsson, M. P.; Hendren, W. R.; Atkinson, R.; Höök, F.; Zayats, A. V.; Polland, R. J. High-Performance Biosensing Using Arrays of Plasmonic Nanotubes. *ACS Nano* **2010**, *4*, 2210–2216.
65. Corthey, G.; Rubert, A. A.; Benitez, G. A.; Fonticelli, M. H.; Salvarezza, R. C. Electrochemical and X-ray Photoelectron Spectroscopy Characterization of Alkanethiols Adsorbed on Palladium Surfaces. *J. Phys. Chem. C* **2009**, *113*, 6735–6742.
66. Marshall, S. T.; O'Brien, M.; Oetter, B.; Corpuz, A.; Richards, R. M.; Schwartz, D. K.; Medlin, J. W. Controlled Selectivity for Palladium Catalysts Using Self-Assembled Monolayers. *Nat. Mater.* **2010**, *9*, 853–858.
67. Chen, P.; Liedberg, B. Curvature of the Localized Surface Plasmon Resonance Peak. *Anal. Chem.* **2014**, *86*, 7399–7405.
68. Wu, C.; Khanikaev, A. B.; Adato, R.; Arju, N.; Yanik, A. A.; Altug, H.; Shvets, G. Fano-Resonant Asymmetric Metamaterials for Ultrasensitive Spectroscopy and Identification of Molecular Monolayers. *Nat. Mater.* **2012**, *11*, 69–75.
69. Mahmoud, M. A. Plasmon Resonance Hybridization of Gold Nanospheres and Palladium Nanoshells Combined in a Rattle Structure. *J. Phys. Chem. Lett.* **2014**, *5*, 2594–2600.
70. Bigelow, N. W.; Vaschillo, A.; Camden, J. P.; Masiello, D. J. Signatures of Fano Interferences in the Electron Energy Loss Spectroscopy and Cathodoluminescence of Symmetry-Broken Nanorod Dimers. *ACS Nano* **2013**, *7*, 4511–4519.
71. Turkevich, J.; Stevenson, P. C.; Hillier, J. A Study of the Nucleation and Growth Processes in the Synthesis of Colloidal Gold. *Discuss. Faraday Soc.* **1951**, *11*, 55–75.
72. Lee, P. C.; Meisel, D. Adsorption and Surface-Enhanced Raman of Dyes on Silver and Gold Sols. *J. Phys. Chem.* **1982**, *86*, 3391–3395.
73. Arakawa, T.; Munaoka, T.; Akiyama, T.; Yamada, S. Effects of Silver Nanoparticles on Photoelectrochemical Responses of Organic Dyes. *J. Phys. Chem. C* **2009**, *113*, 11830–11835.
74. Mätzler, C. *MATLAB Functions for Mie Scattering and Absorption*, Version 2; Institute of Applied Physics University of Bern: Bern, Germany, August **2002**.